Structure and Bonding in Low-spin Octahedral Manganese(II) Carbonyls: Ligand-set Control of Spin Delocalisation *

Gabino A. Carriedo,[a] Neil G. Connelly,[b] Enrique Perez-Carreno,[a] A. Guy Orpen,[b] Anne L. Rieger,[c] Philip H. Rieger,[c] Victor Riera[a] and Georgina M. Rosair[b]

[a] *Department of Organometallic Chemistry, University of Oviedo, Oviedo 33071, Spain*

[b] *School of Chemistry, University of Bristol, Bristol BS8 1TS, UK*

[c] *Department of Chemistry, Brown University, Providence, RI 02912, USA*

X-Ray structural studies on the redox pair *trans*-$[Mn(CN)(CO)(dppm)_2]$ (dppm = $Ph_2PCH_2PPh_2$) and *trans*-$[Mn(CN)(CO)(dppm)_2][PF_6]\cdot CH_2Cl_2$ showed that one-electron oxidation results in changes consistent with depopulation of an orbital involved in Mn–P π-back bonding. The ESR spectra of *trans*-$[Mn(CN)(CO)(dppm)_2]^+$, $[Mn(CO)(CNCH_2CH{=}CH_2)(dppm)_2]^{2+}$, *trans*-$[Mn(CN)(CO)_2(PEt_3)(dppe)]^+$ (dppe = $Ph_2CH_2CH_2PPh_2$) and *trans*-$[MnBr(CO)_2(PEt_3)(dppe)]^+$ in frozen dichloromethane–dichloroethane (1:1) solutions at 90 K, and extended-Hückel molecular-orbital calculations on the model compounds $[Mn(CN)(CO)(H_2PCH_2PH_2)_2]^+$, $[Mn(CO)(CNMe)(H_2PCH_2PH_2)_2]^{2+}$, *cis*- and *trans*-$[Mn(CN)(CO)_2(PH_3)_3]^+$ and *trans*-$[MnBr(CO)_2(PH_3)_3]^+$, showed that the semi-occupied molecular orbital of these low-spin octahedral cyanomanganese(II) carbonyls is always primarily manganese d_π in character and in the plane of the phosphorus ligands, either aligned along the Mn(CN) axis as in *trans*-$[Mn(CO)_2(PEt_3)(dppe)]^+$ or perpendicular to this axis as in *trans*-$[Mn(CN)(CO)(dppm)_2]$. The relative arrangement of the cyanide and carbonyl ligands is shown to control the extent of spin delocalisation onto the cyanide ligand.

It has been known for many years[1] that octahedral manganese(II) carbonyls can be generated by the chemical[2] or electrochemical[3] one-electron oxidation of manganese(I) complexes such as $[MnBr(CO)_{5-n}L_n]$ and $[Mn(CO)_{6-n}L_n]^+$. It is only recently, however, that the chemistry of isolable paramagnetic complexes such as *trans*-$[Mn(CN)(CO)(dppm)_2]^+$ (dppm = $Ph_2PCH_2PPh_2$)[4] and *trans*-$[Mn(CN)(CO)_2\{P(OPh)_3\}(dppm)]^+$[5] has been fully investigated. Thus, the latter is an intermediate in the oxidative isomerisation[5] of *cis*-$[Mn(CN)(CO)_2\{P(OPh)_3\}(dppm)]$ to *trans*-$[Mn(CN)(CO)_2\{P(OPh)_3\}(dppm)]$ and also catalyses[6] the reverse isomerisation process, *i.e. trans* to *cis*. In addition, both types of manganese(II) cyanide complex can be used as ligands in the synthesis of cyano-bridged homo-[7] and hetero-polynuclear[8] redox-active complexes such as **1** and **2**. In order to understand more fully the interactions between the manganese(II) centre(s) and the subsidiary metal- or ligand-based redox sites in such complexes we required a deeper understanding of the bonding in the mononuclear manganese(II) building blocks. We have therefore determined the crystal structures of the redox pair $[Mn(CN)(CO)(dppm)_2]$ **3** and $[Mn(CN)(CO)(dppm)_2]^+$ $\mathbf{3}^+$ (as its $[PF_6]^-$ salt), analysed the anisotropic ESR spectra of the manganese(II) derivatives $\mathbf{3}^+$, $[Mn(CO)(CNCH_2CH{=}CH_2)(dppm)_2]^{2+}$ **4**, *trans*-$[Mn(CN)(CO)_2(PEt_3)(dppe)]^+$ **5** (dppe = $Ph_2PCH_2CH_2PPh_2$), and *trans*-$[MnBr(CO)_2(PEt_3)(dppe)]^+$ **6**, and carried out extended-Hückel molecular orbital (EHMO) calculations on the model compounds $[Mn(CN)(CO)(H_2PCH_2PH_2)_2]^+$ **7**, $[Mn(CO)(CNMe)(H_2PCH_2PH_2)_2]^{2+}$ **8**, *cis*- and *trans*-$[Mn(CN)(CO)_2(PH_3)_3]^+$ **9** and *trans*-$[MnBr(CO)_2(PH_3)_3]^+$ **10**. The results of this combined study provide a detailed picture of the electronic structure of low-spin octahedral manganese(II) carbonyls and the factors which control the delocalisation of the spin density in these species.

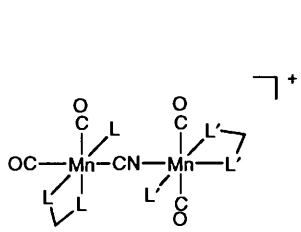

1; L-L, L'-L' = dppm or dppe
L, L' = $P(OPh)_3$, $P(OEt)_3$, or PEt_3

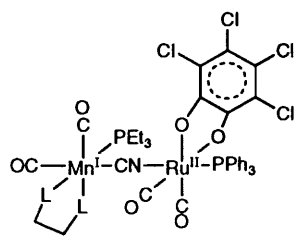

2 L-L = dppe

Results and Discussion

Crystal Structures of $[Mn(CN)(CO)(dppm)_2]^z$ (z = 0 **3** *or* 1 $\mathbf{3}^+$).—The results of the X-ray structure analyses of complexes **3** and $\mathbf{3}^+$ (as a dichloromethane solvate of its $[PF_6]^-$ salt) are summarised in Tables 1 and 2 and illustrated in Figs. 1 and 2. As discussed in the Experimental section, the structure of **3** is subject to an inversion disorder which unfortunately renders the carbonyl and cyanide sites indistinguishable. The structure of $\mathbf{3}^+$ is free from such problems. The co-ordination geometry of **3** is noticeably distorted from regular octahedral with *cis* angles at manganese changed not only because of the small bite angle of the chelating dppm ligands [P(1)–Mn–P(2) 72.5(1)°] but also because of the tilt of the cyanide/carbonyl ligands; the latter are inclined at 6.1° to the MnP_4 plane, hence giving rise to C–Mn–P angles as much as 5.9° from the expected 90°. This distortion may well be a consequence of the chair-like folding (angle between MnP_2 and P_2C planes 28.8°) of the pair of four-

* *Supplementary data available* (No. SUP 56963, 4 pp.): molecular orbital parameters. See Instructions for Authors, *J. Chem. Soc., Dalton Trans.*, 1993, Issue 1, pp. xxiii–xxviii.

Non-SI unit employed: eV ≈ 1.60 × 10^{-19} J.

Table 1 Selected bond lengths (Å) and angles (°) for complex **3**

Mn–C(1)	1.890(2)	C(9)–C(10)	1.388(5)
P(1)–C(3)	1.840(2)	C(11)–C(12)	1.373(4)
P(2)–C(15)	1.852(2)	C(16)–C(17)	1.374(4)
C(1)–O(1)	1.150(3)	C(18)–C(19)	1.362(5)
C(4)–C(5)	1.379(4)	C(22)–C(23)	1.386(3)
C(7)–C(8)	1.405(4)	C(24)–C(25)	1.358(4)
C(10)–C(11)	1.388(4)	Mn–P(2)	2.253(1)
C(13)–C(14)	1.391(4)	P(1)–C(15)	1.853(3)
C(17)–C(18)	1.386(6)	P(2)–C(22)	1.822(2)
C(20)–C(21)	1.393(6)	C(3)–C(8)	1.372(3)
C(23)–C(24)	1.380(3)	C(6)–C(7)	1.361(4)
C(26)–C(27)	1.388(3)	C(9)–C(14)	1.393(3)
Mn–P(1)	2.287(1)	C(12)–C(13)	1.373(5)
P(1)–C(9)	1.835(2)	C(16)–C(21)	1.377(3)
P(2)–C(16)	1.829(3)	C(19)–C(20)	1.351(5)
C(3)–C(4)	1.393(3)	C(22)–C(27)	1.384(3)
C(5)–C(6)	1.360(4)	C(25)–C(26)	1.373(4)
P(1)–Mn–P(2)	72.5(1)	P(1)–Mn–C(1)	95.9(1)
P(2)–Mn–C(1)	93.2(1)	P(1)–Mn–P(1a)	180.0
P(1)–Mn–P(2a)	107.5(1)	P(2)–Mn–P(2a)	180.0
P(1)–Mn–C(1a)	84.1(1)	P(2)–Mn–C(1a)	86.8(1)
C(1)–Mn–C(1a)	180.0	Mn–P(1)–C(3)	129.3(1)
Mn–P(1)–C(9)	121.6(1)	C(3)–P(1)–C(9)	98.8(1)
Mn–P(1)–C(15)	92.8(1)	C(3)–P(1)–C(15)	101.4(1)
C(9)–P(1)–C(15)	109.9(1)	Mn–P(2)–C(15)	93.9(1)
Mn–P(2)–C(16)	127.4(1)	C(15)–P(2)–C(16)	106.5(1)
Mn–P(2)–C(22)	118.0(1)	C(15)–P(2)–C(22)	108.1(1)
C(16)–P(2)–C(22)	101.1(1)	Mn–C(1)–O(1)	177.9(2)

Table 2 Selected bond lengths (Å) and angles (°) for $[Mn(CN)(CO)(dppm)_2][PF_6]\cdot CH_2Cl_2$

Mn–C(1)	1.813(15)	P(1)–C(15)	1.851(13)
Mn–P(2)	2.334(4)	P(2)–C(22)	1.813(9)
N(1)–C(2)	1.146(17)	P(3)–C(40)	1.836(14)
P(1)–C(9)	1.809(12)	P(4)–C(47)	1.812(9)
P(2)–C(16)	1.811(11)	Mn–P(1)	2.345(4)
P(3)–C(34)	1.822(11)	Mn–P(4)	2.351(5)
P(4)–C(41)	1.825(12)	P(1)–C(3)	1.809(9)
Mn–C(2)	1.964(13)	P(2)–C(15)	1.849(14)
Mn–P(3)	2.352(5)	P(3)–C(28)	1.804(10)
O(1)–C(1)	1.133(17)	P(4)–C(40)	1.846(13)
P(1)–Mn–P(2)	73.8(2)	P(1)–Mn–P(3)	104.7(2)
P(2)–Mn–P(3)	178.4(2)	P(1)–Mn–P(4)	174.3(2)
P(2)–Mn–P(4)	108.3(2)	P(3)–Mn–P(4)	73.1(2)
P(1)–Mn–C(1)	91.7(5)	P(2)–Mn–C(1)	88.9(5)
P(3)–Mn–C(1)	91.9(5)	P(4)–Mn–C(1)	93.7(5)
P(1)–Mn–C(2)	88.8(4)	P(2)–Mn–C(2)	92.8(4)
P(3)–Mn–C(2)	86.4(4)	P(4)–Mn–C(2)	85.8(4)
C(1)–Mn–C(2)	178.3(6)	Mn–P(1)–C(3)	123.0(3)
Mn–P(1)–C(9)	117.3(3)	C(3)–P(1)–C(9)	104.5(5)
Mn–P(1)–C(15)	93.1(4)	C(3)–P(1)–C(15)	107.9(5)
C(9)–P(1)–C(15)	109.8(5)	Mn–P(2)–C(15)	93.5(4)
Mn–P(2)–C(16)	125.6(3)	C(15)–P(2)–C(16)	106.5(5)
Mn–P(2)–C(22)	115.5(3)	C(15)–P(2)–C(22)	109.1(5)
C(16)–P(2)–C(22)	105.0(5)	Mn–P(3)–C(28)	120.4(3)
Mn–P(3)–C(34)	125.3(3)	C(28)–P(3)–C(34)	101.1(5)
Mn–P(3)–C(40)	91.7(5)	C(28)–P(3)–C(40)	107.6(5)
C(34)–P(3)–C(40)	108.9(5)	Mn–P(4)–C(40)	91.5(5)
Mn–P(4)–C(41)	120.9(3)	C(40)–P(4)–C(41)	109.9(5)
Mn–P(4)–C(47)	122.1(4)	C(40)–P(4)–C(47)	107.6(5)
C(41)–P(4)–C(47)	103.3(5)	O(1)–C(1)–Mn	175.6(14)
N(1)–C(2)–Mn	179.4(11)		

membered rings in the CP_2MnP_2C system in **3** (see Fig. 1). The opposite sense of the folding in these rings seems to be a general feature of *trans*-$M(dppm)_2$ complexes {*cf.* the structures of $[(dppm)_2(OC)Mn(\mu\text{-}CN)Rh(CO)_2Cl]^z$ for which foldings of 27.2 and 25.2 ($z = 0$) and 27.0 and 23.2° ($z = 1$) are observed [9]} and allows the phenyl rings on the phosphorus atoms to move

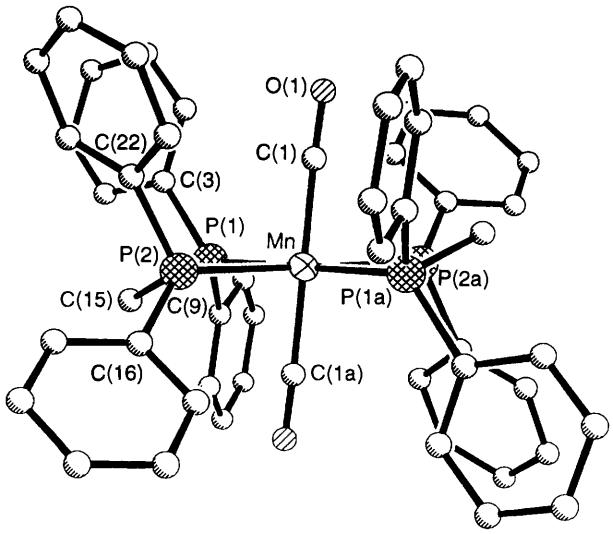

Fig. 1 The molecular structure of complex **3** showing the atom labelling scheme. All hydrogen atoms have been omitted for clarity

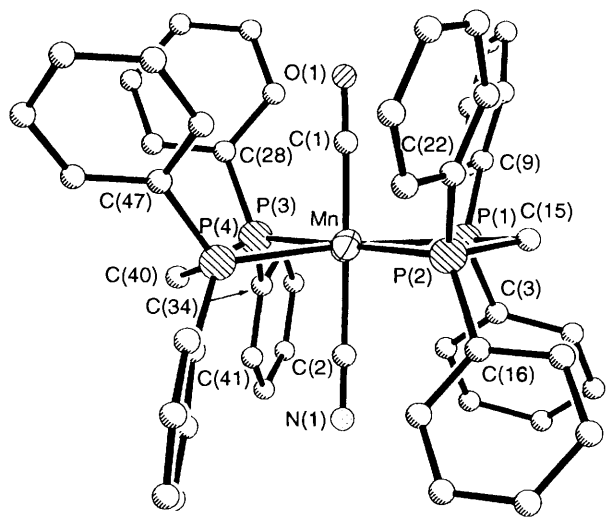

Fig. 2 The molecular structure of complex 3^+ showing the atom labelling scheme. All hydrogen atoms have been omitted for clarity

apart into pseudo-axial and -equatorial sites on the four-membered rings. Folding of saturated four-membered rings (*cf.* cyclobutane) is of course a general feature [10] that is related to relief of torsional strain. The P–Mn–C angular distortion is in the sense which moves the CO/CN ligands towards the less-crowded convex face of the Mn(dppm) rings. We note that such a distortion is undoubtedly variable with the particular values seen for **3** being a consequence of the crystal environment (see 3^+ for less substantial foldings of 8.2 and 22.9°). In solution a range of magnitudes would be expected for the foldings of the $Mn(dppm)_2$ system.

The geometry of complex 3^+ is similar to that of **3** albeit with less strongly folded Mn(dppm) rings and with only approximate $\bar{1}$ symmetry (even ignoring the difference between CN and CO!). The distortion of the octahedral geometry about Mn is also less pronounced in that C–Mn–P angles are closer to 90° (largest deviation 4.2°). There are some aspects of the molecular geometry which have been notably perturbed by oxidation even if some of the details of the changes are inevitably lost due to the disorder in the structure of **3**. The most striking feature is the large increase in the Mn–P distances (mean: **3**, 2.270; 3^+, 2.346 Å) on oxidation, which is accompanied by slight decreases in the average P–C distances (mean $P\text{–}C_{ipso}$ 1.832 and $P\text{–}CH_2$ 1.852 Å for **3**, *cf.* 1.813 and 1.846 Å for 3^+) and increases in the average C–P–C angle (104.3 for **1** to 106.8° for 3^+). These

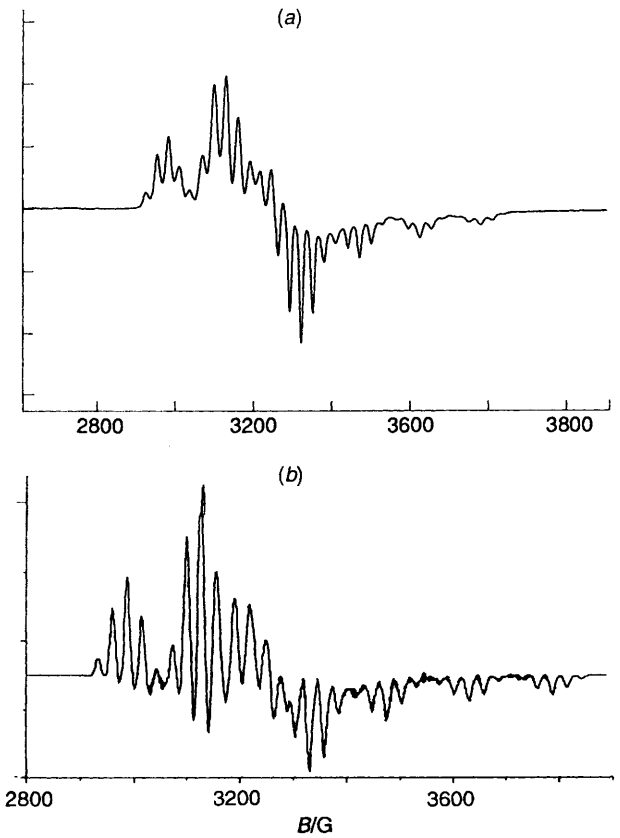

Fig. 3 (*a*) The ESR spectrum of $[Mn(CN)(CO)(dppm)_2]^+$ 3^+ in dichloromethane–dichloroethane (1:1) at 90 K. (*b*) The computer simulation using the parameters of Table 3

changes are similar to those we have observed[11] and discussed[12] for other phosphine-containing redox pairs. They are consistent with depopulation of an orbital involved in Mn–P π-back bonding (see below). In this instance we can use the mean Mn–P distance as a structural measure of the oxidation state of the *trans*-$Mn(CN)(CO)(dppm)_2$ moiety when present as a ligand {*e.g.* in $[(dppm)_2(OC)Mn(\mu\text{-}CN)Rh(CO)_2Cl]^z$ ($z = 0$ and 1)[9]}. Other changes in molecular geometry on oxidation are masked because of the disorder problem.

ESR Spectroscopy.—Isotropic ESR spectra of $[Mn(CN)(CO)(dppm)_2]^+$ 3^+, $[Mn(CO)(CNCH_2CH{=}CH_2)(dppm)_2]^{2+}$ **4** and *trans*-$[Mn(CN)(CO)_2(PEt_3)(dppe)]^+$ **5** were obtained in dichloromethane–1,2-dichloroethane (1:1) solutions at room temperature. With one ^{55}Mn ($I = \frac{5}{2}$) and four ^{31}P ($I = \frac{1}{2}$) nuclei, six 1:4:6:4:1 quintets are expected for 3^+ and **4**. If the three ^{31}P nuclei in **5** are nearly equivalent, six 1:3:3:1 quartets are expected. In fact, only the low-field end of each spectrum was resolved, typically with 8–10 features, but the spectra were readily interpreted assuming that $\langle a^{Mn}\rangle \approx 2\langle a^{P}\rangle$. Reasonably accurate values of $\langle g\rangle$ and $\langle a^{Mn}\rangle$ were obtained but, because the spectra have no well resolved spacing corresponding to $\langle a^{P}\rangle$, the ^{31}P coupling can only be estimated. The isotropic parameters are given in Table 3.

Spectra of complexes 3^+, **4**, **5** and *trans*-$[MnBr(CO)_2(PEt_3)(dppe)]^+$ **6** were also obtained in frozen dichloromethane–dichloroethane (1:1) solutions at 90 K. That of 3^+ is shown in Fig. 3(*a*). The 'parallel' features of the frozen-solution spectra are multiplets (quintets) for 3^+ and **4**, quartets for **5** and **6** (due to coupling of four equivalent or three nearly equivalent ^{31}P nuclei; five of the six features are well separated from the 'perpendicular' features and are easily assigned. Eight to ten 'perpendicular' features are also seen but, since these are superpositions of several components, assignments are not obvious.

In the spectrum of complex 3^+ the spacings between adjacent resolved multiplets is approximately constant, but the average spacing is significantly smaller than one fifth of the $-\frac{5}{2}$ to $+\frac{5}{2}$ spacing. This phenomenon is a manifestation of the non-coincidence of the *g*- and hyperfine-tensor principal axes[13] but, rather than complicating matters, it provides an important aid to the analysis of the spectrum. Assuming that the *g*- and hyperfine-tensor *y* axes are coincident, and making an estimate of A_x^{Mn}, the positions of the 'parallel' features can be fitted to give g_x, g_z, A_z^{Mn}, A^P and the Euler angle β.* The remaining parameters (g_y, A_x^{Mn} and A_y^{Mn}) were fitted by trial and error to give the best fit of a computer simulation to the experimental spectrum. The phosphorus coupling was assumed isotropic, and the fit was guided, but not constrained, by the isotropic parameters using equations (1). The resulting parameters are

$$3\langle g\rangle = g_x + g_y + g_z \quad (1a)$$

$$3\langle A^{Mn}\rangle = A_x^{Mn} + A_y^{Mn} + A_z^{Mn} \quad (1b)$$

given in Table 3 and the computer simulation is shown in Fig. 3(*b*).

Careful examination of the spectra of complexes **4**–**6** shows similar, but smaller, non-coincidence effects, but the angle β is too small to use the above fitting procedure; trial and error therefore played a larger role in the analysis. Although the simulations were in good agreement with the experimental spectra, the *x* and *y* components of the *g* and hyperfine tensors are not as accurately known as the *z* components. Again the phosphorus coupling was assumed isotropic. In the case of **6** the spacings within the 'parallel' quartets are uneven, indicating that one of the couplings is significantly greater than the other two. When reasonable estimates of g_x, g_z, A_x^{Mn} and A_z^{Mn} were available, the 'parallel' features were fitted to give an estimate of β.

Interpretation of ESR Parameters.—Assuming that the *z* axis is perpendicular to the plane of the phosphorus ligands and that the *x* and *y* axes bisect the P–Mn–P bond angles, the semi-occupied molecular orbital (SOMO) is expected to be either d_{xz}, d_{yz} or $d_{x^2-y^2}$ (the t_{2g} set in octahedral symmetry). The fact that the equatorial phosphorus nuclei are equivalent (or nearly so) implies that they are symmetrically arranged with respect to the SOMO, thus ruling out d_{xz} and d_{yz} and leaving $d_{x^2-y^2}$ as the major metal contributor. If the metal contribution to the SOMO is $d_{x^2-y^2}$, g_z should be slightly less than the free-electron value g_e (spin–orbit coupling with d_{xz} and d_{yz} orbitals which lie just below the SOMO). These expectations are in good agreement with experiment.

Thus far the ESR results are in good agreement with qualitative MO theory: the SOMO is expected to be $d_{x^2-y^2}$ since d_{xz} and d_{yz} are involved in π bonding to the axial ligands and thus are stabilised relative to $d_{x^2-y^2}$. However, if the SOMO were solely $d_{x^2-y^2}$, the ^{55}Mn hyperfine tensor should be axial with principal axes identical to those of the *g* tensor. Extended-Hückel MO calculations suggest that the SOMO is indeed predominantly $d_{x^2-y^2}$, but with a small amount of d_{xz} character. As we show below, this is consistent with the rhombic hyperfine tensor and the non-coincident *g*- and hyperfine-tensor principal axes.

If the SOMO has contributions from manganese $d_{x^2-y^2}$ and d_{xz} orbitals, equation (2), the dipolar contributions to the

$$|SOMO\rangle = c_{x^2-y^2}|d_{x^2-y^2}\rangle + c_{xz}|d_{xz}\rangle \quad (2)$$

hyperfine tensor are[14] given by expressions (3a)–(3d). The

* This angle describes the orientation of the hyperfine-tensor principal axes, *x* and *z*, relative to the corresponding *g*-tensor principal axes.

Table 3 The ESR parameters for manganese(II) carbonyl complexes[a]

Complex	$\langle g \rangle$	$\langle A^{Mn} \rangle$[b]	g_x, g_y, g_z	$A_x^{Mn}, A_y^{Mn}, A_z^{Mn}$	β/°	A_x^P, A_y^P, A_z^P
3$^+$	2.0505(2)	59.5(2)	2.048, 2.105, 1.984	20.0, 12.4, 146.1	19.6 ± 0.5	25.7, 25.7, 25.7
4	2.0456(2)	58.6(2)	2.042, 2.102, 1.989	21.0, 7.3, 147.4	7.5 ± 1.0	25.6, 25.6, 25.6
5	2.0463(3)	58.3(2)	2.048, 2.086, 2.004	19.8, 11.0, 144.0	4.6 ± 0.9	24.2, 24.2, 24.2
6			2.044, 2.032, 1.979	27.2, 0, 163.4	6 ± 2	25.2, 25.2, 19.3 (2P) 25.2, 25.2, 27.3 (1P)

[a] Hyperfine couplings in units of 10^{-4} cm^{-1}. [b] $\langle A^P \rangle \approx \langle A^{Mn} \rangle/2$.

Table 4 The SOMO coefficients from ESR parameters for manganese(II) carbonyl complexes

Complex	ρ^d	$(c_{xz})^2$	β_{calc}/°
3$^+$	0.72	0.019	9
4	0.73	0.004	4
5	0.69	0.002	3
6	0.86		

$$A_{xx} = \frac{2}{7}P[(c_{x^2-y^2})^2 + (c_{xz})^2] \quad (3a)$$

$$A_{yy} = \frac{2}{7}P[(c_{x^2-y^2})^2 - 2(c_{xz})^2] \quad (3b)$$

$$A_{zz} = -\frac{4}{7}P\left[(c_{x^2-y^2})^2 - \frac{1}{2}(c_{xz})^2\right] \quad (3c)$$

$$A_{xz} = \frac{6}{7}P(c_{x^2-y^2})(c_{xz}) \quad (3d)$$

matrix is diagonalised by rotation about the y axis by the angle β, equation (4), to give the principal values in equations (5a) and (5b). Assuming that the d_{xz} contribution is small and including

$$\tan 2\beta_A = 2c_{xz}/c_{x^2-y^2} \quad (4)$$

$$A_{x'} = \frac{2}{7}P\left[(c_{x^2-y^2})^2 + 4(c_{xz})^2 - \frac{3(c_{xz})^4}{(c_{x^2-y^2})^2}\right] \quad (5a)$$

$$A_{z'} = -\frac{4}{7}P\left[(c_{x^2-y^2})^2 + (c_{xz})^2 - \frac{3(c_{xz})^4}{2(c_{x^2-y^2})^2}\right] \quad (5b)$$

the spin–orbit coupling contributions, we have expressions (6) and (7) where $\Delta g_i = g_i - g_e$ and $P = 207.6 \times 10^{-4}$ cm^{-1}.[15]

$$A_{z'} - \langle A \rangle = P\left\{-\frac{4}{7}[(c_{x^2-y^2})^2 + (c_{xz})^2] + \frac{2}{3}\Delta g_z + \frac{5}{42}(\Delta g_x + \Delta g_y)\right\} \quad (6)$$

$$A_{x'} - A_y = P\left[\frac{12}{7}(c_{xz})^2 + \frac{17}{14}(\Delta g_x - \Delta g_y)\right] \quad (7)$$

The d-electron spin densities, $\rho^d = (c_{x^2-y^2})^2 + (c_{xz})^2$, computed using equation (6), are given in Table 4, along with values of $(c_{xz})^2$ and β, computed using equations (7) and (4), respectively.

The values of β estimated using equations (7) and (4) are about half those obtained from analysis of the spectra, perhaps because of errors in the experimental x and y components or failure of the theory. More likely, however, the principal axes of the g tensor are also rotated from the reference cartesian axes. Neglecting delocalisation of spin density into ligand orbitals, the components of the g tensor are given[13] by equations (8a)–(8d) where ζ_{Mn} is the manganese spin–orbit coupling parameter,

$$g_{xx} = g_e + 2\zeta_{Mn}\sum_{m\neq 0}\frac{(c_{x^2-y^2}c_{yz}^m + c_{xz}c_{xy}^m)^2}{E_0 - E_m} \quad (8a)$$

$$g_{yy} = g_e + 2\zeta_{Mn}\sum_{m\neq 0}\frac{[c_{x^2-y^2}c_{xz}^m + c_{xz}(\sqrt{3}c_{z^2}^m - c_{x^2-y^2}^m)]^2}{E_0 - E_m} \quad (8b)$$

$$g_{zz} = g_e + 2\zeta_{Mn}\sum_{m\neq 0}\frac{(2c_{x^2-y^2}c_{xy}^m + c_{xz}c_{yz}^m)^2}{E_0 - E_m} \quad (8c)$$

$$g_{xz} = -2\zeta_{Mn}\sum_{m\neq 0}\frac{(c_{x^2-y^2}c_{yz}^m + c_{xz}c_{xy}^m)(2c_{x^2-y^2}c_{xy}^m + c_{xz}c_{yz}^m)}{E_0 - E_m} \quad (8d)$$

E_0 is the energy of the SOMO, E_m the energy of the mth molecular orbital, and c_{xy}^m (for example) is the linear combination of atomic orbitals (LCAO) coefficient of d_{xy} in the mth molecular orbital.

In a simple ligand-field theory model, we would expect d_{xy} to be at high energy and d_{yz} and d_{xz} to be just below the SOMO. Thus we expect g_{xx} and g_{yy} to be significantly larger than g_e. This expectation is supported by experiment and by the EHMO calculations; a MO with a large d_{yz} contribution is predicted about 1.0 eV below the SOMO. From the ligand-field theory model, we expect g_{zz} to be slightly less than g_e, but the EHMO calculations give MOs containing large contributions from d_{xy}, about 6.2 eV above and 4.0 eV below the SOMO. These cancel to some extent, but still lead to a positive contribution.

If we assume that no MO contains appreciable amounts of both d_{yz} and d_{xy} character, the expressions for the g-tensor components can be simplified to (9a)–(9c) where δ_k is given by equation (10). To this level of approximation, and with

$$g_{xx} = g_e + (c_{x^2-y^2})^2\delta_{yz} + (c_{xz})^2\delta_{xy} \quad (9a)$$

$$g_{zz} = g_e + 4(c_{x^2-y^2})^2\delta_{xy} + (c_{xz})^2\delta_{yz} \quad (9b)$$

$$g_{xz} = -(c_{x^2-y^2})(c_{xz})(\delta_{yz} + 2\delta_{xy}) \quad (9c)$$

$$\delta_k = 2\zeta_{Mn}\sum_{m\neq 0}\frac{(c_k^m)^2}{E_0 - E_m} \quad (10)$$

$c_{xz} \ll c_{x^2-y^2}$, the principal axes are rotated in the xz plane by the angle β_g [equation (11)] and, if $|\delta_{xy}/\delta_{yz}| \ll 1$, as expected

$$\tan 2\beta_g = -\frac{2c_{xz}}{c_{x^2-y^2}}\frac{1 + (2\delta_{xy}/\delta_{yz})}{1 - (4\delta_{xy}/\delta_{yz})} \quad (11)$$

from the simple ligand-field model and qualitatively supported by the EHMO calculations, we would have $\beta_g = -\beta_A$, doubling the non-coincidence effect. Since the analysis of the hyperfine components accounts for about half of the non-coincidence, this is precisely what is expected.

There are two potential sources of error. First, although EHMO calculations show that MOs rarely have both d_{xy} and

d_{yz} character, there are a few exceptions, close in energy to the SOMO. When amplified by a small energy denominator, these contributions might be significant. Secondly, the expressions for the *g*-tensor components given above do not include contributions from ligand orbitals; unfortunately, the theory of the *g* tensor has not been developed to the point where off-diagonal elements can be estimated accurately for delocalised systems,[16] even with reliable wavefunctions.

The metal contribution to the SOMO is about 72% for complexes 3^+ and **4** with two equatorial dppm ligands, 69% for **5** with dppe, PEt_3 and cyanide ligands, and 85% for **6** with dppe, PEt_3 and bromide ligands. If we assume that there is no spin density on Br or the axial ligands, *i.e.* that the only significant delocalisation is onto phosphorus, then we have a contribution of *ca.* 5% per phosphorus atom. Assuming the same contribution of the phosphorus atoms in **5**, we have a cyanide ligand contribution of *ca.* 16%. A similar argument applied to 3^+ and **4** (allowing 5% per phosphorus and 0% for the axial ligands) accounts for 92% of the spin. An important distinction between dppm and dppe or monodentate phosphines is the overlap of the methylene carbon orbitals with metal-based orbitals in dppm complexes; $\rho^C \approx 0.04$ is not an unreasonable estimate for the contribution of carbon $2p_x$ to the SOMO.

Extended-Hückel Molecular-orbital Calculations.—The EHMO calculations[17] were made on the model compounds $[Mn(CN)(CO)(H_2PCH_2PH_2)_2]^+$ **7**, $[Mn(CO)(CNMe)(H_2PCH_2PH_2)_2]^{2+}$ **8**, *cis*- and *trans*-$[Mn(CN)(CO)_2(PH_3)_3]^+$ **9**, and *trans*-$[MnBr(CO)_2(PH_3)_3]^+$ **10**. In all cases the axial ligands (CO, CN or CNMe) were placed on the *z* axis and the *x* and *y* axes bisected the equatorial ligand bonds. Parameters used in the calculations and the idealised bond lengths and angles have been deposited as SUP 56963. The results of these calculations are summarised in Table 5 which gives charge-matrix compositions for the SOMO in **7**–**10**.

The ESR spectroscopic results suggested that the SOMO in the manganese(II) complexes is primarily $d_{x^2-y^2}$ in character, but with a significant d_{xz} admixture to account for the non-coincidence of the *g*- and hyperfine-tensor principal axes. From these results the SOMO was estimated to have about 70% manganese 3d character in the cyanide and isocyanide complexes, about 85% in the bromide complex. In the EHMO calculations we sought to test the ability of this semi-quantitative method to reproduce these experimental features and to understand their origin.

The calculated SOMO for each of complexes **7**–**10** is primarily Mn $3d_{x^2-y^2}$, in accord with the ESR analysis. This d_π orbital is uniquely high in energy because it lies in the plane containing three or four phosphine ligands in every case. Only for *cis*-**9** is there a strong π-acceptor ligand (CO) in this plane. In view of our interest in the ability of such manganese(II) species to act as ligands *via* a bridging cyanide ligand it is of particular interest that while **7** (or *cis*-**9**) shows essentially no delocalisation of spin onto the cyanide ligand, *trans*-**9** shows significant delocalisation of this sort. This divergent behaviour arises because the $d_{x^2-y^2}$ SOMO is δ with respect to the Mn–CN axis in **7** (and *cis*-**9**) but π in *trans*-**9**. The implication is that real $Mn^{II}(CN)$ complexes (such as **5**), with analogous ligand sets and stereochemistry to those of *trans*-**9**, will act as more effective transmitters of π-spin density through μ-CN ligands than will analogues of **7** (such as 3^+).

We now turn to more quantitative aspects of the EHMO analysis. With the $H_2PCH_2PH_2$ (diphosphinomethane, dpm) groups in the plane normal to the axial ligands (C_{2v} symmetry), the metal contribution to the SOMO of complex **7** is necessarily strictly $d_{x^2-y^2}$ with no d_{xz} admixture. The only other significant contribution to the SOMO is an antibonding admixture of *ca.* 4% carbon $2p_x$ from each of the bridging methylene groups of the dpm ligands. The other metal d_π orbitals are stabilised by interaction with the axial π-acid ligands and hence, as noted above, $d_{x^2-y^2}$ is uniquely high in energy. Distortions of the geometry of **7** to an asymmetric structure based on the crystal structure of 3^+, and of both **7** and **8** to C_s geometries† yielded SOMOs with small (< 2%) d_{xz} contributions (see Table 5).

In all these calculations the SOMO of complex **7** was about 89% metal 3d, substantially greater than the 72% estimated from the ESR analysis. The largest additional atomic orbital

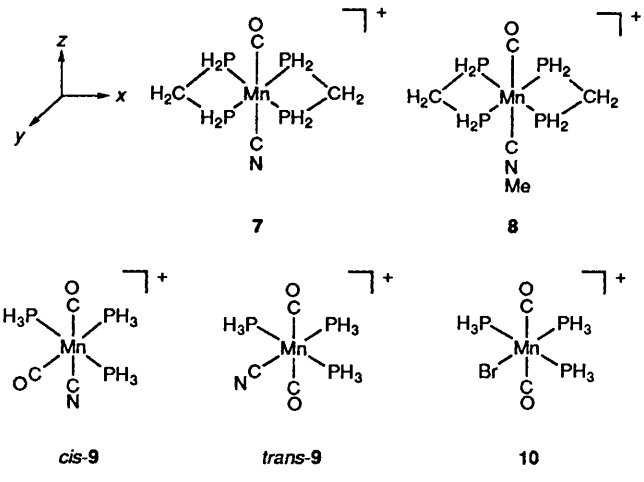

Table 5 The SOMO charge-matrix composition (in electrons) from extended-Hückel MO calculations

Structure	H_{ii}*	Mn	Other atoms
7 C_{2v}	—	$d_{x^2-y^2}$ 0.892	C(H_2) p_x 0.041
X-ray coordinates	—	$d_{x^2-y^2}$ 0.896	C(H_2) p_x 0.026, 0.035
		d_{xz} 0.005	C(H_2) p_z 0.005, 0.000
C_s	—	$d_{x^2-y^2}$ 0.861	C(H_2) p_x 0.033, 0.042
		d_{xz} 0.018	C(H_2) p_z 0.006, 0.005
	−4.0	$d_{x^2-y^2}$ 0.714	C(H_2) p_x 0.044, 0.056
		d_{xz} 0.028	C(H_2) p_z 0.008, 0.007
		d_{z^2} 0.003	P d_{xy} 0.014, 0.015
	−6.0	$d_{x^2-y^2}$ 0.601	C(H_2) p_x 0.053, 0.067
		d_{xz} 0.037	C(H_2) p_z 0.009, 0.008
		d_{z^2} 0.008	P d_{xy} 0.026, 0.029
			P $d_{x^2-y^2}$ 0.004, 0.005
8 C_s	—	$d_{x^2-y^2}$ 0.860	C(H_2) p_x 0.042, 0.033
		d_{xz} 0.019	C(H_2) p_z 0.005, 0.006
	−4.0	$d_{x^2-y^2}$ 0.712	C(H_2) p_x 0.044, 0.056
		d_{xz} 0.030	C(H_2) p_z 0.008, 0.007
			P d_{xy} 0.014, 0.015
9 *trans*	—	$d_{x^2-y^2}$ 0.809	C(N) p_x, p_y 0.012
			N p_x, p_y 0.038
	−4.0	$d_{x^2-y^2}$ 0.666	C(N) p_x, p_y 0.007
			N p_x, p_y 0.039
			P d_{xy} 0.038, 0.035
cis	—	$d_{x^2-y^2}$ 0.703	C(O) p_x, p_y 0.048
		d_{xz} 0.010	O p_x, p_y 0.034
		d_{yz} 0.010	
	−4.0	$d_{x^2-y^2}$ 0.383	C(O) p_x, p_y 0.023, 0.012
		d_{xz} 0.015	O p_x, p_y 0.020, 0.011
		d_{yz} 0.015	C(N) p_x, p_y 0.002
			N p_x, p_y 0.018
			P $d_{x^2-y^2}$ 0.022, 0.022
			P d_{xz} 0.000, 0.014
10	—	$d_{x^2-y^2}$ 0.784	Br p_x, p_y 0.075
	−4.0	$d_{x^2-y^2}$ 0.582	Br p_x, p_y 0.119
			P $d_{x^2-y^2}$ 0.028, 0.024

* Phosphorus 3d coulomb integral.

† The phosphorus and bridging carbon atoms were moved ± 0.125 and ± 0.662 Å, respectively, out of the plane normal to the axial ligands; the distortions were approximately that of the more distorted group in the crystal structure.

contribution comes from the $2p_x$ orbitals of the bridging carbon atoms of the dpm ligands; phosphorus orbitals contributed less than 0.1%. One way of forcing greater phosphorus contribution in the SOMO is to invoke the participation of phosphorus 3d orbitals. We began with a phosphorus 3d coulomb integral (H_{ii}) of −6.0 eV, as suggested by Hoffmann *et al.*[18] The result was a significant delocalisation onto phosphorus, reducing the metal participation to 65%. A better fit to the ESR analysis is obtained with a phosphorus 3d coulomb integral of −4.0 eV, whereupon the metal contribution is 74% (d_{xz} contribution 2.8%). Note that the inclusion of the phosphorus 3d orbitals amplifies the effect of equatorial ring distortion on the incorporation of d_{xz} character in the SOMO, bringing the calculations into still closer conformity to the ESR results. Taken together these results are in qualitative agreement with a model of phosphine back bonding we have previously described[11,12] in which the π-acceptor function of a tertiary phosphine is composed of a mixture of P–C σ* and P 3d orbitals. The actual composition as calculated by EHMO is of course highly dependent on both the coulomb integrals employed and the geometry at phosphorus.

Calculations on complex **8** gave results very similar to those from **7**, in agreement with the similar ESR results for $\mathbf{3}^+$ and **4** (Table 5).

On the basis of the calculations the *cis* isomer of complex **9** is predicted to be the more stable for a d^6 manganese(I) electron count by 0.10 eV (0.044 eV if phosphorus 3d orbitals are included) whereas the *trans* isomer is, as expected, calculated to be the more stable for a d^5 manganese(II) electron count, by 0.18 eV (0.19 eV when P 3d orbitals are included). This result is consistent with the fact that the *cis* isomer of $[Mn(CN)(CO)_2L(dppe)]$ [L = PR_3 or $P(OR)_3$] is the more thermally stable, but only the *trans* isomer of the related manganese(II) cations, $[Mn(CN)(CO)_2L(dppe)]^+$, is known.

The calculated composition of the SOMO of *trans*-**9** (for a phosphorus 3d coulomb integral set to −4.0 eV) is in satisfactory agreement with that obtained from the ESR analysis of the spectrum of complex **5**; again the metal contribution was substantially greater when phosphorus 3d orbitals were not included.

Calculations on complex **10** showed significant contributions of the bromine $3p_x$ and $3p_y$ orbitals to the SOMO which resulted in a reduction of the metal character to well below that expected from the ESR results. The calculated net charge on bromine was −0.17 or −0.31, depending on whether phosphorus 3d orbitals were or were not included. In the cases of *cis*- and *trans*-**9**, the SOMO involves the participation of the π-acceptor ligands CO and CN^-. In contrast, in **10** the bromine ligand acts as a weak π donor and as a result destabilises the SOMO. This is reflected in the calculated energies of the SOMOs. Thus for *cis*-**9**, for which the strongest π acceptor (CO) is in the equatorial plane, this energy is −11.99 eV; in *trans*-**9**, with the moderate π-acceptor CN in the equatorial plane, the energy is higher (−11.70 eV), and for **10** it is higher still (−11.25 eV). It would seem from the comparison between ESR and EHMO results that the bromine atomic orbital parameters are rather crude approximations which lead to unreasonably large bromine contributions to the SOMO. Making the coulomb integral parameters and Slater exponents more negative and larger, respectively, would bring the two approaches into closer accord. Indeed, Hoffmann and co-workers[19] appear to have similar troubles with chlorine parameters, judging from the changes made in successive papers.

Conclusion

A combination of X-ray crystallography, ESR spectroscopy, and EHMO theory calculations has provided a unified picture of the electronic structure of low-spin octahedral cyano-

Table 6 Structure analyses*

	3	$\mathbf{3}^+PF_6^-\cdot CH_2Cl_2$
Crystal data		
Formula	$C_{52}H_{44}MnNOP_4$	$C_{53}H_{46}Cl_2F_6MnNOP_5$
M	877.7	1107.6
Crystal system	Monoclinic	Orthorhombic
Space group	*C*2/*c* (no. 15)	$Pna2_1$ (no. 33)
a/Å	24.493(7)	22.470(6)
b/Å	9.639(4)	11.935(4)
c/Å	21.851(6)	19.279(6)
β/°	122.92(2)	90
U/Å^3	4330(2)	5170(3)
D_c/g cm^{-3}	1.34	1.42
F(000)	1824	2268
μ(Mo-Kα)/cm^{-1}	4.9	5.7
Data collection and reduction		
Crystal dimensions (mm)	0.7 × 0.7 × 0.6	0.5 × 0.3 × 0.2
Colour	Orange	Dark red
Scan method	ω–2θ	Wyckoff, ω
Scan width, ω	1.0 + $\Delta\alpha_1\alpha_2$	0.6
Total data	5177	5423
Unique data	3925	4693
'Observed' data [$F^2 > 2\sigma(F^2)$], N_o	3164	2928
No. azimuthal scan data	410	424
Minimum, maximum transmission coefficients	0.845, 0.880	0.515, 0.618
Refinement		
Least-squares variables, N_v	269	271
R	0.032	0.074
R'	0.038	0.069
S	1.62	1.67
Final difference map features (e Å^{-3})	+0.22, −0.18	+0.59, −0.41

* Details in common: *T* 295 K; *Z* = 4; crystals from CH_2Cl_2–hexane; 2θ 4–50°. $R = \Sigma|\Delta|/\Sigma|F_o|$; $R' = (\Sigma w\Delta^2/\Sigma wF_o^2)^{\frac{1}{2}}$; $S = [\Sigma w\Delta^2/(N_o - N_v)]^{\frac{1}{2}}$; $\Delta = F_o - F_c$; $w = [\sigma_c^2(F_o) + 0.0005F_o^2]^{-1}$, $\sigma_c^2(F_o)$ = variance in F_o due to counting statistics.

Table 7 Atomic coordinates ($\times 10^4$) for complex **3**

Atom	*x*	*y*	*z*	Atom	*x*	*y*	*z*
Mn	0	0	0	C(13)	1899(1)	−3991(3)	962(1)
P(1)	113(1)	−2109(1)	−399(1)	C(14)	1275(1)	−3485(2)	686(1)
P(2)	−769(1)	−1417(1)	−83(1)	C(15)	−345(1)	−3020(2)	−68(1)
C(1)	−570(1)	760(2)	−938(1)	C(16)	−985(1)	−1659(2)	590(1)
O(1)*	−903(1)	1255(2)	−1503(1)	C(17)	−1460(1)	−2579(3)	478(2)
N(1)*	−903(1)	1255(2)	−1503(1)	C(18)	−1623(2)	−2723(4)	991(2)
C(3)	−287(1)	−2777(2)	−1335(1)	C(19)	−1312(1)	−1959(3)	1616(2)
C(4)	−225(1)	−4184(2)	−1431(1)	C(20)	−844(1)	−1049(3)	1736(2)
C(5)	−510(1)	−4755(3)	−2118(2)	C(21)	−681(1)	−885(3)	1221(1)
C(6)	−862(1)	−3940(3)	−2717(1)	C(22)	−1571(1)	−1400(2)	−927(1)
C(7)	−941(1)	−2569(3)	−2639(1)	C(23)	−1939(1)	−215(2)	−1057(1)
C(8)	−657(1)	−1970(3)	−1943(1)	C(24)	−2550(1)	−82(3)	−1685(2)
C(9)	914(1)	−2920(2)	−12(1)	C(25)	−2797(1)	−1113(3)	−2190(1)
C(10)	1196(1)	−2867(3)	−416(1)	C(26)	−2440(1)	−2293(3)	−2079(1)
C(11)	1815(1)	−3393(3)	−142(2)	C(27)	−1825(1)	−2437(3)	−1449(1)
C(12)	2162(1)	−3955(3)	545(2)				

* Occupancy 0.5.

Table 8 Atomic coordinates ($\times 10^4$) for complex $3^+PF_6^-\cdot CH_2Cl_2$

Atom	*x*	*y*	*z*	Atom	*x*	*y*	*z*
Mn	8 313(1)	7 550(2)	10 000	C(22)	8 260	10 311	10 630
P(1)	9 101(1)	8 101(3)	9 279(3)	C(23)	7 944(4)	10 379(7)	11 252(5)
P(2)	8 745(1)	9 108(3)	10 530(3)	C(24)	7 496	11 178	11 331
P(3)	7 904(2)	5 968(3)	9 450(3)	C(25)	7 364	11 909	10 788
P(4)	7 578(1)	6 835(3)	10 746(3)	C(26)	7 679	11 842	10 166
P(5)	10 747(2)	1 791(4)	9 874(3)	C(27)	8 127	11 043	10 087
F(1)	11 362(6)	1 796(16)	9 650(15)	C(28)	7 326	6 127	8 808
F(2)	10 091(5)	1 761(13)	10 117(12)	C(29)	7 349(3)	7 008(6)	8 333(6)
F(3)	10 846(8)	2 893(13)	10 235(12)	C(30)	6 917	7 096	7 817
F(4)	10 652(7)	685(12)	9 568(12)	C(31)	6 462	6 304	7 775
F(5)	10 568(14)	2 337(28)	9 306(13)	C(32)	6 439	5 424	8 250
F(6)	10 918(16)	1 290(25)	10 481(14)	C(33)	6 871	5 335	8 767
O(1)	7 468(4)	9 086(8)	9 323(6)	C(34)	8 328	4 808	9 087
N(1)	9 170(5)	5 887(10)	10 738(7)	C(35)	8 643(4)	4 067(8)	9 510(5)
C(1)	7 801(6)	8 482(13)	9 558(8)	C(36)	9 011	3 258	9 212
C(2)	8 857(5)	6 502(10)	10 464(8)	C(37)	9 064	3 189	8 492
C(3)	9 784	7 309	9 198	C(38)	8 749	3 930	8 070
C(4)	10 331(4)	7 861(5)	9 184(6)	C(39)	8 381	4 739	8 368
C(5)	10 857	7 246	9 138	C(40)	7 550(6)	5 504(10)	10 259(7)
C(6)	10 837	6 079	9 104	C(41)	7 741	6 558	11 657
C(7)	10 290	5 527	9 118	C(42)	7 548(4)	7 339(7)	12 147(6)
C(8)	9 763	6 142	9 164	C(43)	7 704	7 211	12 843
C(9)	8 918	8 503	8 400	C(44)	8 053	6 304	13 049
C(10)	8 999(4)	7 708(6)	7 878(5)	C(45)	8 245	5 523	12 560
C(11)	8 798	7 927	7 207	C(46)	8 089	5 650	11 864
C(12)	8 517	8 941	7 057	C(47)	6 830	7 402	10 770
C(13)	8 437	9 736	7 579	C(48)	6 342(4)	6 708(5)	10 893(6)
C(14)	8 638	9 517	8 251	C(49)	5 780	7 173	10 996
C(15)	9 263(6)	9 366(10)	9 802(7)	C(50)	5 705	8 333	10 975
C(16)	9 193	9 084	11 311	C(51)	6 193	9 027	10 851
C(17)	9 569(4)	9 986(6)	11 448(5)	C(52)	6 756	8 562	10 749
C(18)	9 906	10 005	12 056	C(53)	4 701(8)	11 372(16)	11 348(10)
C(19)	9 866	9 120	12 527	Cl(1)	4 003(3)	12 009(4)	11 256(4)
C(20)	9 489	8 217	12 390	Cl(2)	4 828(4)	10 901(8)	12 183(4)
C(21)	9 153	8 199	11 781				

manganese(II) carbonyls. The SOMO of such species is always primarily manganese d_π in character aligned in the plane of the phosphorus donors, the weakest π-acceptor ligands in the examples studied here. As a consequence, the SOMO is orientated either along the Mn(CN) axis, as in **5** (or the model complex *trans*-**9**), or perpendicular to this axis, as in 3^+ (or the model complexes **7** or *cis*-**9**). This opens the way to the rational design of polynuclear complexes where spin delocalisation from manganese(II) to a second metal, *via* a cyanide bridge, may be controlled by the systematic manipulation of the stereochemistry at manganese.

Experimental

The complexes $[Mn(CN)(CO)(dppm)_2]$, $[Mn(CN)(CO)(dppm)_2][PF_6]$,[8b] $[Mn(CO)(CNCH_2CH{=}CH_2)(dppm)_2]^+$,[20] *trans*-$[Mn(CN)(CO)_2(PEt_3)(dppe)]^+$[5] and *trans*-$[MnBr(CO)_2(PEt_3)(dppe)]$[2a] were prepared by published methods. Samples for ESR spectroscopy were prepared under an atmosphere of dry nitrogen, using dried, distilled and deoxygenated solvents. The ESR spectra were recorded on a Bruker ESP-300E spectrometer, equipped with a Bruker variable-temperature accessory and a Hewlett-Packard 5350B microwave frequency counter. The field calibration was checked by measuring the

resonance of the diphenylpicrylhydrazyl (dpph) radical before each series of spectra.

Structure Determinations of Complexes **3** *and* 3^+ *(as a Dichloromethane Solvate of its* $[PF_6]^-$ *Salt).*—Many of the details of the structure analyses carried out on complexes **3** and 3^+ (as a dichloromethane solvate of its $[PF_6]^-$ salt) are listed in Table 6. X-Ray diffraction measurements on single crystals mounted in thin-walled glass capillaries were made with graphite-monochromated Mo-Kα X-radiation ($\bar{\lambda}$ = 0.710 73 Å) using Siemens four-circle *P3m* diffractometers. Cell dimensions for each analysis were determined from the setting angle values of 38 and 40 centred reflections respectively in the range $14 < 2\theta < 30°$.

Intensity data were collected for unique portions of reciprocal space and corrected for Lorentz, polarisation, crystal decay (of 70% for 3^+), long-term intensity fluctuations and absorption effects, the latter on the basis of azimuthal scan data. The structures were solved by heavy atom (Patterson and Fourier difference) methods, and refined by full-matrix least squares against *F*. For complex **3** all non-hydrogen atoms were assigned anisotropic displacement parameters and refined without positional constraints. The model used for **3** requires that the cyanide and carbonyl groups are disordered since the molecule sits at a site of $\bar{1}$ symmetry and a single atomic site was assigned for the oxygen and nitrogen atoms each with 50% occupancy. Therefore the position and dimensions reported in Tables 1 and 7 for the carbonyl oxygen O(1) refer also to N(1).

The choice of space group for complex 3^+ was based on the intensity statistics ($< E^2 - 1 > = 0.78$), which are consistent with a non-centrosymmetric space group, and on successful solution refinement in $Pna2_1$. Disordered $Pna2_1$ models were investigated for which the N and O sites were exchanged or mixed nitrogen and oxygen occupancies for the sites reported in the tables were refined (*i.e.* to probe possible disorder of the sort seen for **3**). The oxygen and nitrogen occupancies refined to unity within experimental uncertainties. Thus the most satisfactory model as judged by these latter refinements, residual indices and chemical reasonableness was the ordered one reported in Table 8, for which no correlation coefficients > 0.5 between heavy (*i.e.* Mn, P) atom parameters were observed. Phenyl groups were constrained to idealised geometries (planar, C–C 1.395 Å, C–C–C 120°). All atoms heavier than carbon, and carbon atoms C(1) and C(2), were assigned anisotropic displacement parameters and refined without constraints. All other carbon atoms were assigned freely refined isotropic displacement parameters. The absolute structure given in Table 8 was assigned on the (somewhat ambiguous) basis of a Rogers η refinement[23] [η = 0.6(3)]. In both analyses all hydrogen atoms were assigned fixed isotropic displacement parameters and were constrained to ideal geometries with C–H 0.96 Å.

Final difference syntheses showed no chemically significant features, the largest maxima being close to the metal atoms. Refinements converged smoothly to residuals given in Table 6. Tables 7 and 8 report the positional parameters for the non-hydrogen atoms. All calculations were made with programs of the SHELXTL-PLUS[22] system as implemented on a Siemens R3m/V structure determination system. Complex neutral-atom scattering factors were taken from ref. 23.

Additional material available from the Cambridge Crystallographic Data Centre comprises H-atom coordinates, thermal parameters and remaining bond lengths and angles.

Acknowledgements

We thank the SERC for a Studentship (to G. M. R.) and for funds to purchase an ESR spectrometer, and the British Council and Spanish Ministry of Education and Science for an Accion Integrada grant. We thank Dr. D. M. Proserpio for useful discussions.

References

1 N. G. Connelly and W. E. Geiger, *Adv. Organomet. Chem.*, 1984, **23**, 18 and refs. therein.
2 (*a*) F. Bombin, G. A. Carriedo, J. A. Miguel and V. Riera, *J. Chem. Soc., Dalton Trans.*, 1981, 2049; (*b*) R. H. Reimann and E. Singleton, *J. Chem. Soc., Dalton Trans.*, 1973, 2658; (*c*) P. M. Treichel, G. E. Dirreen and H. J. Mueh, *J. Organomet. Chem.*, 1972, **44**, 339.
3 A. M. Bond, R. Colton and M. E. McDonald, *Inorg. Chem.*, 1978, **17**, 2842 and refs. therein.
4 G. A. Carriedo, V. Riera, N. G. Connelly and S. J. Raven, *J. Chem. Soc., Dalton Trans.*, 1987, 1769.
5 N. G. Connelly, K. A. Hassard, B. J. Dunne, A. G. Orpen, S. J. Raven, G. A. Carriedo and V. Riera, *J. Chem. Soc., Dalton Trans.*, 1988, 1623.
6 N. G. Connelly, S. J. Raven, G. A. Carriedo and V. Riera, *J. Chem. Soc., Chem. Commun.*, 1986, 992.
7 G. A. Carriedo, N. G. Connelly, M. C. Crespo, I. C. Quarmby, V. Riera and G. H. Worth, *J. Chem. Soc., Dalton Trans.*, 1991, 315; G. A. Carriedo, N. G. Connelly, S. Alvarez, E. Perez-Carreno and S. Garcia-Granda, *Inorg. Chem.*, 1993, **32**, 272.
8 (*a*) G. Barrado, G. A. Carriedo, C. Diaz-Valenzuela and V. Riera, *Inorg. Chem.*, 1991, **30**, 4416; (*b*) A. Christofides, N. G. Connelly, H. J. Lawson, A. C. Loyns, A. G. Orpen, M. O. Simmonds and G. H. Worth, *J. Chem. Soc., Dalton Trans.*, 1991, 1595; (*c*) A. Christofides, N. G. Connelly, H. J. Lawson and A. C. Loyns, *J. Chem. Soc., Chem. Commun.*, 1990, 597.
9 F. L. Atkinson, A. Christofides, N. G. Connelly, H. J. Lawson, A. C. Loyns, A. G. Orpen, G. M. Rosair and G. H. Worth, *J. Chem. Soc., Dalton Trans.*, 1993, 1441.
10 J. D. Dunitz, *X-Ray Structure Analysis and the Structure of Organic Molecules*, Cornell University Press, Ithaca, NY, 1979, p. 423ff.
11 N. G. Connelly, M. J. Freeman, A. G. Orpen, A. R. Sheehan, J. B. Sheridan and D. A. Sweigart, *J. Chem. Soc., Dalton Trans.*, 1985, 1019; A. G. Orpen, N. G. Connelly, M. W. Whiteley and P. Woodward, *J. Chem. Soc., Dalton Trans.*, 1989, 1751.
12 A. G. Orpen and N. G. Connelly, *J. Chem. Soc., Chem. Commun.*, 1985, 1310; *Organometallics*, 1990, **9**, 1206.
13 R. D. Pike, A. L. Rieger and P. H. Rieger, *J. Chem. Soc., Faraday Trans. 1*, 1989, 3913; P. H. Rieger, in *Organometallic Radical Processes*, ed. W. C. Trogler, Elsevier, Amsterdam, 1990, ch. 8.
14 B. M. Peake, P. H. Rieger, B. H. Robinson and J. Simpson, *J. Am. Chem. Soc.*, 1980, **102**, 156.
15 J. R. Morton and K. F. Preston, *J. Magn. Reson.*, 1977, **30**, 577.
16 A. J. Stone, *Proc. R. Soc. London, Ser. A*, 1963, **271**, 424.
17 R. Hoffmann, *J. Chem. Phys.*, 1963, **39**, 1397; J. Howell, A. Rossi, D. Wallace, I. K. Harak and R. Hoffmann, *Quantum Chemistry Program Exchange*, 1977, **10**, 344; C. Mealli and D. M. Proserpio, *J. Chem. Educ.*, 1990, **67**, 399.
18 R. Hoffmann, J. M. Howell and E. L. Muetterties, *J. Am. Chem. Soc.*, 1972, **94**, 3047.
19 R. H. Summerville and R. Hoffmann, *J. Am. Chem. Soc.*, 1976, **98**, 7240; 1979, **101**, 3821; T. A. Albright, P. Hofmann and R. Hoffmann, *J. Am. Chem. Soc.*, 1977, **99**, 7546.
20 N. G. Connelly, A. G. Orpen, G. M. Rosair and G. H. Worth, *J. Chem. Soc., Dalton Trans.*, 1991, 1851.
21 D. Rogers, *Acta Crystallogr., Sect. A*, 1981, **37**, 734.
22 G. M. Sheldrick, SHELXTL-PLUS Rev. 4.1, Göttingen, 1990.
23 *International Tables for X-Ray Crystallography*, Kynoch Press, Birmingham, 1974, vol. 4.

Received 29*th March* 1993; *Paper* 3/01809A